International Journal of Heat and Mass Transfer 157 (2020) 119891

Contents lists available at ScienceDirect

International Journal of Heat and Mass Transfer

journal homepage: www.elsevier.com/locate/hmt

A new method for heat transfer coefficient measurements of single-phase fluids during laminar flow in microchannels ☆

Seungwhan Baek*, Ray Radebaugh, Peter E. Bradley

Material Measurement Laboratory, National Institute of Standards and Technology, 325 Broadway, Boulder, Colorado 80305, United States

ARTICLE INFO

Article history:
Received 26 September 2019
Revised 8 April 2020
Accepted 27 April 2020

Keywords:
Heat transfer coefficient
Microchannel
Axial conduction
Single-phase
Laminar flow

ABSTRACT

The measurement of heat transfer coefficients in microchannels is complicated due to the small sizes involved. Moreover, a heat transfer mechanism which is not usually considered, the axial conduction effect in the channel wall, must also be evaluated in micro-scale measurements. Previous heat transfer coefficient measurements have not accounted for the axial conduction effect, and those measurements showed the inconsistent result with the theory. In this paper, a new measurement method is developed to validate the theory that predicts a Nusselt number independent of Reynolds number in the laminar flow regime for microchannels. A numerical model is used to simulate heat transfer characteristics in a microchannel with wall conduction, and to predict the wall temperature difference between a location at the end of the heater and a location 3 mm away from the heater on the microchannel. The temperature difference is experimentally measured on a 160 μm hydraulic diameter microchannel and compared with the numerical model. The comparison shows that the Nusselt number in the laminar flow regime for the microchannel is independent of Reynolds number at least down to Re=300.

1. Introduction

The heat transfer coefficient (h) between a solid and a fluid is essential information for the development of heat transfer devices, such as heat exchangers. Information regarding heat transfer coefficient characteristics is usually obtained from correlations derived from experiments or theory. It is well-known that the Nusselt number (Nu) in the laminar regime is constant [1], and the heat transfer coefficient in the turbulent flow regime is usually expressed by the Gnielinski equation [2-4] or Dittus-Boelter equation [5] for macrochannel applications. The recent development of microchannel devices, such as microchannel heat exchangers, requires correlations of the heat transfer coefficient from the microscale perspective. The measurement of heat transfer coefficients has been ongoing for several decades. However, unlike macrochannel research, microchannel measurements show inconsistent results among researchers [6], especially in the laminar flow regime.

The measurement of heat transfer coefficient starts with measuring wall and fluid temperatures at the same position along the flow channel. Thermocouples are attached to the wall and inserted inside the tube to measure the fluid temperature separately. However, it is difficult to measure the fluid temperature in microchannels, because thermocouple sizes are usually larger than the inner diameter of the microchannel. To overcome this difficulty, previous researchers used indirect methods to estimate heat transfer coefficients. Wu and Little [7] first measured the heat transfer coefficients of nitrogen in trapezoidal microchannels. One pair of the counterflow microchannel heat exchanger is utilized to measure the heat transfer coefficient. They measured fluid temperature in the larger channels before entering the microchannel heat exchanger. Choi et al. [8] presented Nusselt numbers with respect to Reynolds numbers from measurements in microchannels, where Nusselt number and Reynolds number are defined by Eqs. (1) and (2), respectively

$$Nu_x = \frac{h_x D_h}{k_f} \tag{1}$$

$$\mathrm{Re}_x = \frac{\rho V D_h}{\mu_f} = \frac{G D_h}{\mu_f} \tag{2}$$

In Eqs. (1) and (2), D_h is the hydraulic diameter of the channel, k_f is the thermal conductivity of the fluid, ρ is the density of the fluid, V is the velocity of the fluid, and μ_f is the viscosity of the fluid. The G is the mass flux which is the rate of the mass flow per unit area ($\dot{m}/A$).

For the experimental case of Choi et al [8], the microchannel was surrounded by a constant temperature fluid. Four thermocou-

☆ Contributions of NIST, not subject to copyright in the United States.

* Corresponding author at: Launcher Propulsion System Team, KSLV-II R&D Head Office, Korea Aerospace Research Institute, 169-84, Gwahak-ro, Yuseong-gu, Daejeon, 34133, South Korea

E-mail addresses: sbaek@kari.re.kr (S. Baek), ray.radebaugh@nist.gov (R. Radebaugh), peter.bradley@nist.gov (P.E. Bradley).

https://doi.org/10.1016/j.ijheatmasstransfer.2020.119891
0017-9310/

Nomenclature

A	heat transfer area (m^2)
A_c	cross-sectional area of fluid flow (m^2)
B	total bias error
c_p	heat capacity (J(/kg•K))
D_h	hydraulic diameter (m)
G	mass flux (kg/(s•m^2))
h	heat transfer coefficient (W/(m^2•K))
k	thermal conductivity (W/(m•K))
L	length (m)
$\dot{m}$	mass flow rate (kg/s)
N	number of data
Nu	Nusselt number
p	pressure (Pa)
q	heat rate (W)
Re	Reynolds number
S	standard deviation
T	temperature (K)
$t_{95\%}$	T-distribution for a confidence level
th	thickness (m)
U	uncertainty
x	length (m)

Subscripts

f	fluid
HT	heat transfer area
in	inlet
out	outlet
w	wall
x	position

Greek letters

μ	viscosity (Pa-s)

ples were attached on the outside wall of the microchannel, and the inlet and outlet fluid temperatures were measured before and after the microchannel. Peng and Peterson [9] measured the heat transfer coefficients of water flowing in microchannels constructed between microchannel plates. Six thermocouples were attached on the wall of the channels. Additional thermocouples were installed in the plenums at the entrance and exit to measure the inlet and outlet liquid temperature. Morini et al. [10] measured the heat transfer coefficient of nitrogen gas in a microchannel of D_h=172 μm. Five thermocouples were attached to the wall of the channel, and additional thermocouples were inserted into the plenums to measure the fluid temperature at the inlet and the outlet of the microchannel.

The measurement methods in the above four studies are different from each other and show inconsistent results. Fig. 1 shows the different results of Nusselt numbers from measurements and correlations from the preceding research. Table 1 summarizes the correlations and experimental conditions from previous researchers.

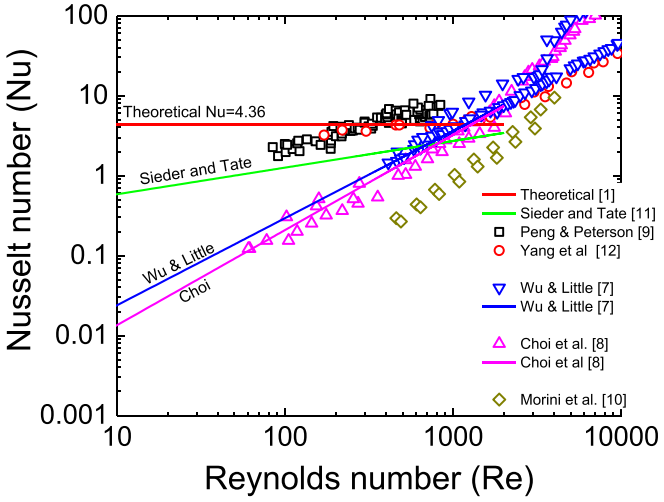

Fig. 1. The Nusselt numbers from past measurements and theory.

Fig. 1 shows the inconsistency of Nusselt numbers from past measurements and theory for microchannels briefly. Theoretically, the Nusselt number may indicate 4.36 in the circular micro-tube within the laminar flow regime [1]. However, the Sider and Tate correlation [11] show lower values than 4.36 at Reynolds numbers below 2000. The experimental Nusselt numbers from Wu and little [7] and Choi et al. [8] indicate values less than 1 for Reynolds numbers less than 1000. The experimental value from Morini[10] shows a similar trend compared to past research. However, there also exist different experimental Nusselt number values from Peng and Peterson [9], and Yang [12], where their results show values from 1 to 10 in the laminar flow regime.

None of the studies show constant Nusselt number for Reynolds numbers below 2000 (laminar flow regime). The above studies all showed reduced Nusselt numbers in the laminar flow regime. The previous studies were limited because they could not measure the actual fluid temperature inside the microchannel to estimate the heat transfer coefficient accurately.

Later, as Maranzana et al. [13] indicated, the axial conduction affects traditional heat transfer coefficient measurements in the microscale regime. Maranzana et al. concluded that inaccurate fluid temperature estimation based on inlet and outlet temperatures results in underestimation of the Nusselt number in the laminar flow regime. Lin and Kandlikar [14] derived a correlation that predicts Nusselt number reduction with traditional heat transfer analysis. Maranzana et al. [13] proposed measurement techniques for the actual fluid temperature in the microchannels using non-invasive measurement techniques, such as infrared thermography. However, such measurements were not carried out. Yang et al. [12] introduced a new technique to measure the surface temperature of the microchannel but neglected axial conduction in the analysis. Recently, Baek et al. [15] experimentally investigated the Nusselt number in the low Reynolds number with traditional heat transfer coefficient measurements.

Table 1
Selected literature for single-phase laminar heat transfer.

Author	Condition	Correlation or remarks
Sieder and Tate [11]	-Circular channel-Simultaneously developing	$Nu = 1.86(\frac{Re\,Pr\,D_h}{L})^{1/3}(\frac{\mu_f}{\mu_w})^{0.14}$
Wu & Little [7]	- Rectangular(trapezoidal) channel, nitrogen gas, D_h=156 μm, 153 μm	$Nu = 0.00222Re^{1.09}Pr^{0.4}$
Choi et al. [8]	- circular channel (experimental), nitrogen gas, D_h=9.7 μm, 53 μm, 81.2 μm	$Nu = 0.000972Re^{1.19}Pr^{1/3}$
Morini et al. [10]	- Circular channel (experimental), nitrogen gas, D_h=172 μm, 750 μm	- no correlation, observed reduction of Nu
Yang et al. [12]	- Circular channel (experimental), air, D_h=920 μm, 308 μm, 86 μm	- no correlation, observed Nu decreasing tendency
Peng et al. [9]	- Rectangular channel (experimental), water, D_h=150 ~343 μm	$Nu = 0.1165(\frac{D_h}{W_c})^{0.81}(\frac{H}{W})^{-0.79}Re^{0.62}Pr^{1/3}$

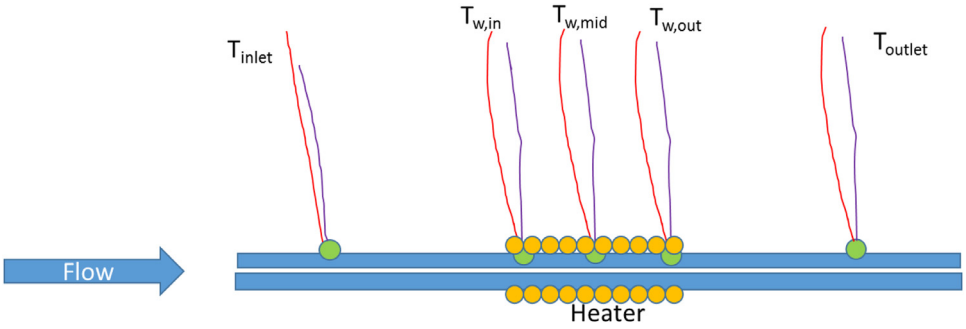

Fig. 2. Thermometer installation on the microchannel: the thermometer size is larger than the microchannel and can't be installed inside the microchannel.

In this paper, we present a new microscale measurement method that takes axial conduction into account. The new method derived from a numerical model analysis. This proposed new method is discussed and validated with experimental measurements.

2. Development of the new measurement method

The basic heat transfer coefficient measurement requires fluid temperature and wall temperature at the same (x) position. The measurement limitation for microchannel applications is that conventional thermometers are physically larger in size (~200 μm) than the channel size (~100 μm) they must be inserted. Therefore, it is impossible to measure the fluid temperature inside the channel directly. Alternatively, thermometers can be installed either 1) on the outside of the microchannel or 2) in the fluid at the larger inlet and the outlet sections (manifolds) leading into and out from of the microchannel. The latter thermometer installation is not recommended, because the fluid temperature at those locations do not represent the fluid temperature in the microchannel.

For this reason, the installation of thermometers on the outside of the microchannel is the only feasible technique. Consequently, thermocouples can be installed in the heating regions and non-heating regions on the microchannel, as shown in Fig. 2. Additionally, the temperature difference between such thermometers can be obtained from the measurement. To determine which information is useful for heat transfer coefficient analysis, a simulation of wall temperature profile along the microchannel, including the axial conduction effect is required at this stage.

A one-dimensional numerical approximation of the microchannel heat transfer model that includes the axial conduction effect is developed here [15, 16]. This model is composed of the fluid channel and two surrounding walls, as displayed in Fig. 3. The numerical technique proceeds by identifying control volumes and placing nodes (i.e., temperatures predicted at each location). The arrangement of nodes and control volumes are shown in Fig. 3. The numerical solution is enabled by carrying out an energy balance on each of the control volumes identified in Fig. 3. The governing relations for the energy balance of the fluid streams and the channel walls are given by Eqs. (3) and (4).

$$\dot{m}c_p\frac{dT_f}{dx} = -\left(\frac{h_1A_{HT,1}}{L}\right)(T_f - T_{w,1}) - \left(\frac{h_2A_{HT,2}}{L}\right)(T_f - T_{w,2}) \quad (3)$$

$$\frac{d}{dx}\left(k_{w,1}A_{c,w,1}\frac{dT_{w,1}}{dx}\right) + \frac{d}{dx}\left(k_{w,2}A_{c,w,2}\frac{dT_{w,2}}{dx}\right) = \dot{m}c_p\frac{dT_f}{dx} \quad (4)$$

Subscripts 1 and 2 denote the upper wall and lower wall, respectively. A_{HT} is the heat transfer area between the wall and fluid, and A_c is the cross-sectional area of the wall.

Numerical techniques for similar heat transfer models with axial conduction are fully described in the literature [16]. Only critical elements will be highlighted in this paper. The model input parameters are:

- heat transfer coefficient between the wall and fluid (h).
- thickness (th_w) and thermal conductivity (k_w) of the wall.
- mass flow rate ($\dot{m}$), inlet temperature (T_{in}), heat capacity (c_p) and thermal conductivity (k_f) of the fluid.
- channel height (D_h), width (W), heated length (L).
- heat transfer area (A_{HT}) and cross-sectional area of channel ($A_{c,w}$) calculated from the channel geometry.
- heat input to the channel (q).

Table 2
Simulation parameter for sensitivity analysis.

Parameter	Value
Wall thermal conductivity	stainless steel: 16 W/m•K, ideal wall: 0 W/m•K
Fluid thermal conductivity	0.026 W/m•K
Fluid viscosity	18.5×10^{-6} Pa/s
Heating Length	3 cm
Total length	3 cm
inlet temperature	300 K
Inner diameter	110 μm
Outer diameter	310 μm
Heat input	0.05 W
Nusselt number	4.36

The pressure drop in the microchannel is neglected in this numerical model as thermophysical property differences are usually negligible for pressure changes in laminar flow. The output results from the microchannel heat transfer model are the temperature profile of the fluid and the wall. Validation of the model development is described in previous works [15, 17]. The simulation used nitrogen gas properties using REFPROP 9 [18].

Table 2 presents the model geometry. Two wall conditions are considered in the numerical model: the ideal wall and the actual wall. The thermal conductivity for the ideal wall is zero, whereas the actual wall's thermal conductivity is 16 W/m•K, which represents a grade 304 stainless steel microchannel tube. The temperature profiles are in dimensionless form (Eq. (5)) as:

$$T(\Theta) = \frac{T_{x(wall\ or\ fluid)} - T_{f,in}}{T_{f,out} - T_{f,in}} \quad (5)$$

Fig. 4 (a) shows the simulated temperature profiles of the wall and fluid for the actual and the ideal condition. In this case, the Reynolds number is 90, which represents a low flowrate compared to Re=2000. The Nusselt number is 4.36. When the thermal conductivity of the wall is zero, the fluid and the wall temperature show linear temperature profiles along the length of the channel, which are depicted with red lines. On the other hand, the fluid and the wall temperature increase non-linearly when the thermal conductivity of the wall is high, (16 W/m•K) as discussed in previous studies [13, 17], and are depicted with black lines in Fig. 4.

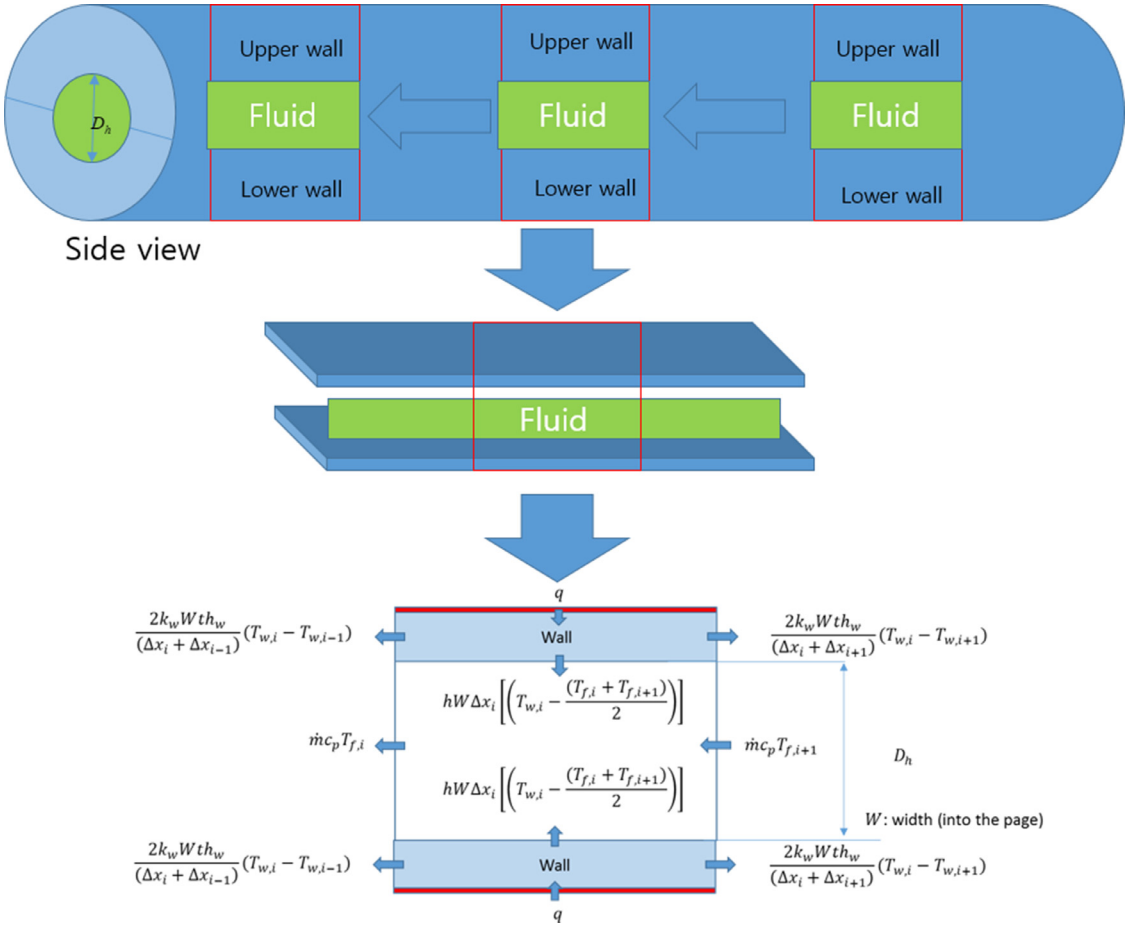

Fig. 3. 1-D simulation basis.

The temperature difference between the wall and the fluid is constant when the thermal conductivity of the wall is zero. However, it is not constant for the actual condition (16 W/m•K). The inlet temperature difference (ΔT_{in}=$T_{w,in}$-$T_{f,in}$) is relatively large, and the outlet temperature difference (ΔT_{out}=$T_{w,out}$-$T_{f,out}$) is small.

For comparison, the Nusselt number is reduced to 1 in Fig. 4 (b), when the Reynolds number is 90. Arbitrarily, a decreased Nusselt number is selected based on previous measurements showing Nusselt numbers to be less than 4.36 [7, 8]. From Fig. 4 (b), it can be observed that the shapes of the temperature profiles are not different from the previous condition. However, the inlet and the outlet temperature difference increases when compared to the case of Nu=4.36.

The axial conduction also affects the measurement error. In Fig. 4 (a), when there is no axial conduction both fluid and wall temperatures (red lines) are linear along the length of the microchannel. Measuring the inlet and outlet fluid temperatures, assuming axisymmetry along the channel, the temperature at the mid-pt is determined from averaging the inlet and outlet fluid temperatures. When axial conduction exists the temperature profile of both the fluid and wall become non-linear as the black lines show. Measuring only inlet and outlet fluid temperatures leads to misrepresentation of the actual fluid temperature and thus a poor determination of the non-linear fluid temperature profile along the microchannel. For calculation of the heat transfer coefficient, it is essential to know the fluid temperature. The existence of axial conduction affects the fluid temperature as shown in Fig. 4. This difference between the actual fluid temperature and the calculated temperature leads to error in the heat transfer coefficient calculation.

The inlet and outlet temperature differences show noticeable change when the Nusselt number or the heat transfer coefficient is varied. If the inlet and outlet temperature differences are measured in the experiment, the heat transfer coefficient can be determined by comparing the temperature differences from the experiment to the simulation. The next step is to investigate the sensitivity of the inlet and outlet temperature differences to the thermal conductivity and the heat transfer coefficient.

The non-dimensional inlet and outlet temperature differences are calculated when the thermal conductivity of the wall is varied from 1 to 2000 W/m•K for the geometry given in Table 2. These values are calculated for three values of Reynolds number: 22, 441, and 1766. Fig. 5 (a) shows the calculation results. The dimensionless inlet temperature difference converges to 1 when the thermal conductivity of the wall increases. The high wall thermal conductivity changes the wall condition from constant heat flux to constant wall temperature condition. The outlet temperature difference decreases by three orders of magnitude when the wall thermal conductivity increases and when the Reynolds number is 22. For higher Reynolds numbers, the temperature difference does not change so rapidly with conductivity change.

The change of the inlet and outlet temperature difference is calculated with the model when the heat transfer coefficient is varied from 1 to 2000 W/m^{2}K. The thermal conductivity is set as 16 W/m•K for this case. Fig. 5 (b) depicts the results. When the Reynolds number is low i.e. 22, the outlet temperature difference shows a change of eight orders of magnitude. The outlet temperature difference increases as the Reynolds number increases, but it still changes by three orders of magnitude. The inlet tempera-

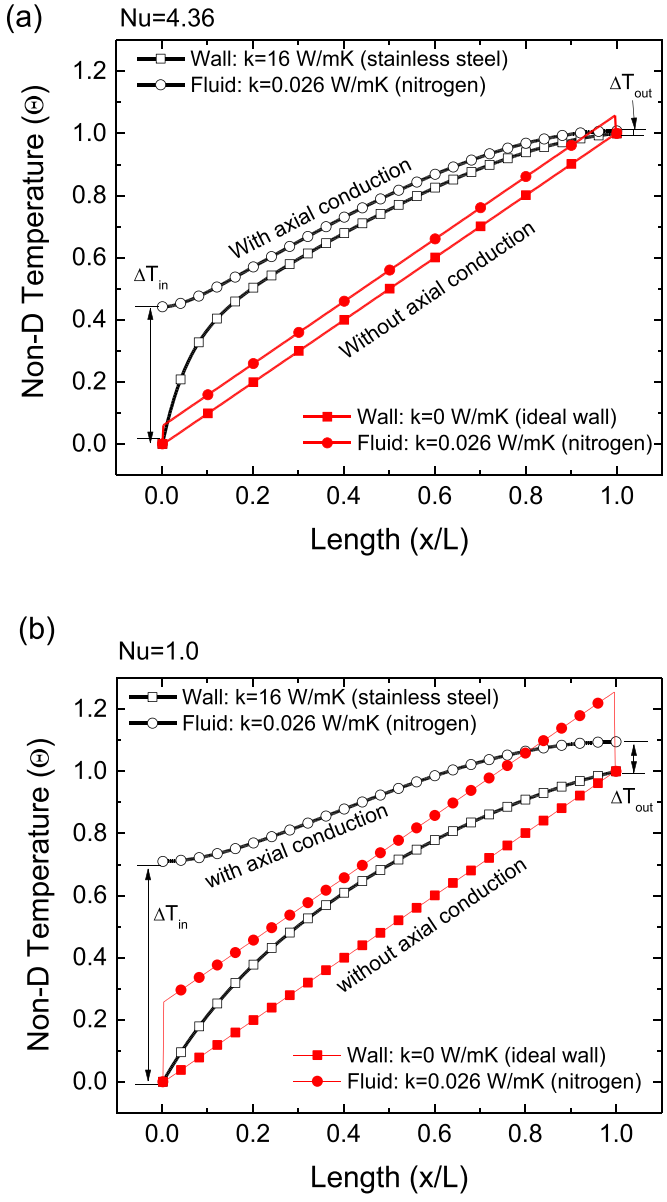

Fig. 4. Temperature profile of wall and fluid (a) when the Nu=4.36 (b) when the Nu=1.0.

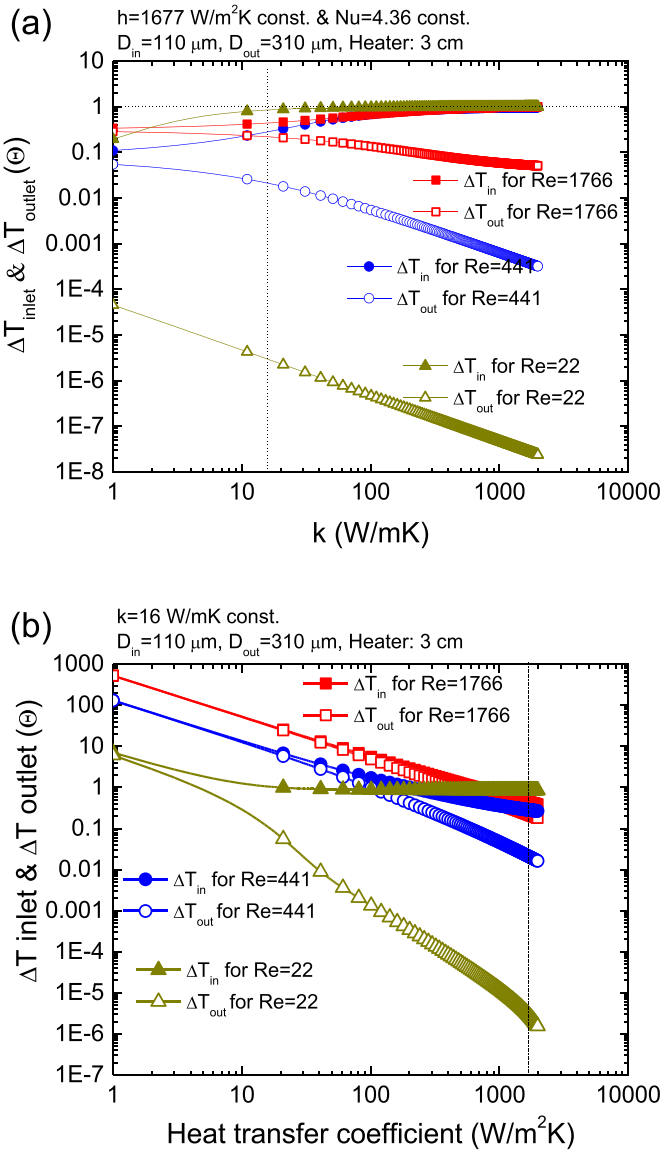

Fig. 5. Sensitivity analysis for temperature differences between wall and fluid, when the heating length is 3 cm for: (a) the change in thermal conductivity (b) the change in heat transfer coefficient.

ture difference does not show as much change as that of the outlet temperature difference.

Fig. 5 discusses the temperature difference between the wall and fluid at the inlet and the outlet. For example, the blue empty circle line in Fig. 5 (a) indicates the temperature difference ($\Delta T_{out} = T_{w.out} - T_{f.out}$) between the wall and the fluid at the channel outlet. If one changes the material of the microchannel, where thermal conductivity of the channel will change (such as glass, stainless steel, copper), the ΔT_{out} will also change. However, that change in ΔT_{out} value with material substitution is not significant where thermometers may not detect low ΔT_{out} values.

The blue empty circle line in Fig. 5 (b) shows the temperature difference between fluid and wall for change in heat transfer coefficient (change in Nusselt number). If Nusselt number decreases as from other previous research, the ΔT_{out} will change significantly, unlike Fig. 5 (a).

If the Nusselt number does not change, ΔT_{out} may change as the Reynolds number changes, shown as red, blue, and brown lines. Therefore, if one considers the change in Nusselt number with respect to the change in Reynolds number in the laminar flow regime, it is better to observe the temperature difference between the wall and fluid at the outlet of the microchannel.

From a comparison of Fig. 5 (a) and (b), the outlet temperature difference (ΔT_{out}) shows a greater change with the heat transfer coefficient than with the wall thermal conductivity. Therefore, the measurement of the outlet temperature difference can be an alternative approach to determine the heat transfer coefficient between the fluid and the wall. If the outlet temperature difference is measured with various Reynolds numbers in laminar flow and compared to the results in Fig. 5 (b), the heat transfer coefficient can be determined by comparing calculations from measurement and simulation. However, the temperature differences between wall and fluid in Fig. 5 (a) and (b) are extremely small, on the order of 0.0001 K. Such differences should be increased for the actual measurement by changing the geometry and the heat input.

In the next section, the paper presents an approach to increase the outlet temperature difference and the measurement technique.

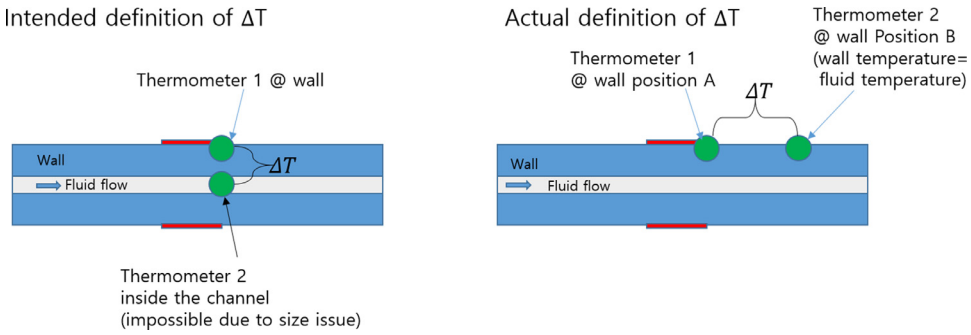

Fig. 6. Definition of ΔT_{out} in the experiment.

Table 3
Microchannel geometry for the experiment and the numerical model.

Parameter	Value
Length	90 mm
Heating length	5 mm
Inner diameter (D_{in})	160 μm
Outer diameter (D_{out})	310 μm
Material	Stainless steel 304

3. Experimental technique

In the previous section, the outlet temperature difference between the fluid and the wall is discussed. However, it is not feasible to measure the temperature of the fluid in the microchannel due to mismatch in temperature sensor and channel size. This section provides methods to distinguish heat transfer characteristics by measuring different wall temperatures on the microchannel, despite the above limitation.

Measurement of the outlet temperature difference ($\Delta T_{out} = T_{w,out} - T_{f,out}$) should be precise and accurate to compare with the simulation. But this temperature difference decreases to a very small value when the Reynolds number is low. To magnify the outlet temperature difference, the heating length should be decreased, and the heating power should be increased. Moreover, the axial conduction effects exist not only in the heating region but also at the non-heating region in the microchannel.

The numerical model is thus revised to consider the heating region and the non-heating region. Table 3 presents geometry information for the model. The model provides the temperature at all locations for both the wall and the fluid that is used to determine the region where the wall temperature (beyond the heating region) decays to nearly that of the fluid temperature.

The wall temperature at different positions is measured to realize the temperature difference between the wall and fluid. Fig. 6 shows the definition for the outlet temperature difference ΔT_{out} for the experiment and analysis.

Initially, ΔT_{out} should be the actual temperature difference between the fluid and the solid wall. However, in microscale, current measurement capability does not allow direct measurement of the fluid temperature. Therefore, measurement of wall temperatures at different locations is conducted. Surely, wall temperature at the heater is the wall temperature. Furthermore, the exterior wall temperature a distance after the heater or non-heated section is equal to the fluid temperature. Thus, the wall temperature at the non-heated part is the fluid temperature. Therefore, the temperature difference from wall to fluid $\Delta T = T_{wall} - T_{fluid}$ is determined from $\Delta T = T_{wall\ @\ heater\ end} - T_{wall\ @\ heater\ end+x\ mm}$.

A trial and error method with the numerical model is applied to determine the heated length of the channel and the heating power. The objective of the test is to obtain a significant temperature difference between the heater and the non-heated section. The short heating length and high heating power assure a high outlet temperature difference between the wall and fluid. Because of the axial conduction effect, if the heated length is long, as if along the entire channel length, the temperature will be similar at two locations. Therefore, the heated length should be much shorter than the entire channel length, and the heating power should be higher. In this paper, the channel length is 70 mm, and the heating length is determined to be 5 mm. Heating power of 70 mW and greater was determined sufficient to establish a significant temperature difference between the end of the heater and 3 mm away.

During the trial and error simulations, the Nusselt number is fixed at 4.36 for the investigation. Fig. 7 (a) shows the temperature profile of the fluid and the wall with a high Reynolds number of 1354. The inlet temperature is 301 K. Two cases of wall thermal conductivity values are shown in the figure. When the wall thermal conductivity is zero, the wall temperature rises only at the heated zone (thin red lines). The thick black lines demonstrate the influence of k values (k_w=16 W/m•K) for the stainless steel microchannels employed. Note the large temperature rise occurring along the 5 mm length heated zone. The wall temperature and the fluid temperature become identical a distance of about 5 mm away from the heated zone.

Fig. 7 (b) shows the temperature profiles of the wall and fluid for the low Reynolds number case (Re=180). The inlet temperature is 303 K. The ideal wall case (k_w=0 W/m•K) also shows that the wall temperature rises only at the heated zone. However, for the actual wall case (k_w =16 W/m•K), the temperature rise of the outlet wall is not as significant as the ideal wall case or as with the case of high Reynolds number. Due to the axial conduction effect, the inlet wall part shows a significant temperature increase. The outlet temperature difference between the wall and fluid is less than with the case for high Reynolds number, as discussed above.

Since the thermocouple size is larger than the hydraulic diameter of the microchannel, the actual outlet temperature difference between the wall and fluid cannot be measured. However, the wall temperature right after the heated zone and the wall temperature at a distance 3 mm away from the heated zone can be measured and compared to the simulation to determine the heat transfer coefficient. The measurement location of ΔT on the microchannel is indicated in Fig. 7 (a) and (b). Additional thermocouples should be installed on the microchannel after the heated zone, to determine the final outlet temperature of the microchannel, as indicated in Fig. 7.

Fig. 8 shows the comparison of temperature measurement methodologies (macroscale versus microscale) to determine the heat transfer coefficients. Fig. 8 (a) shows the measurement placement for the macrochannel. The channel scale permits thermometers to be installed inside the macrochannel, where fluid and the inner wall temperature can be measured directly. Fig. 8 (b) shows

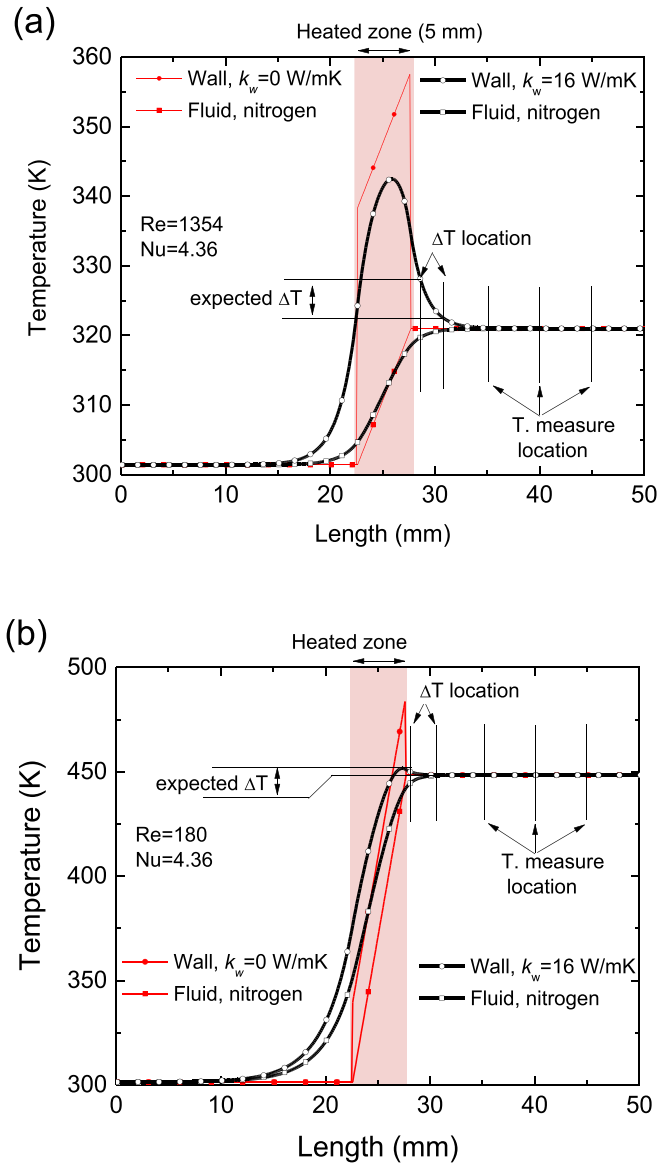

Fig. 7. Simulation of wall and fluid temperature profile in the microchannel (a) high Reynolds number (b) low Reynolds number.

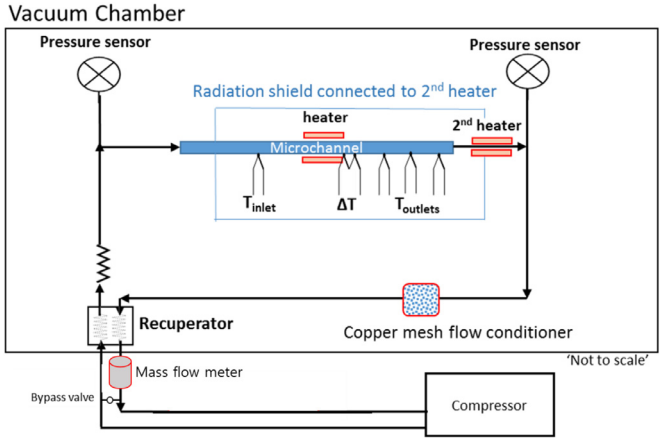

Fig. 9. Experimental setup for the heat transfer coefficient measurement in the microchannel.

the traditional temperature measurement method for microchannels. Thermometers are positioned before and after the microchannel to measure the inlet and outlet fluid temperatures. The temperature of the fluid located at the mid-point of the channel is estimated assuming a linear temperature profile and anchored from the exterior wall temperature measurement at the mid-point between the fluid temperature measurements. Fig. 8 (c) shows the proposed temperature measurement method for microchannels to determine the heat transfer coefficient calculation. Two thermometers are utilized in the analysis. One thermometer is located at the end of the heater to measure the highest wall temperature. The second thermometer is situated a distance away from the heater, where the fluid and the wall temperature are equal. The temperature difference is then obtained for a given fixed distance along the channel.

4. Experimental setup

Fig. 9 displays the schematic of the experimental setup for measurement of the heat transfer coefficient of a fluid in a microchannel. The gaseous nitrogen circulates around the experimental setup in a closed-loop manner. The setup includes an oil-less compressor that resides outside of the vacuum chamber. The microchannel test section resides inside the vacuum chamber for the experiment. In operation, compressed nitrogen from the compres-

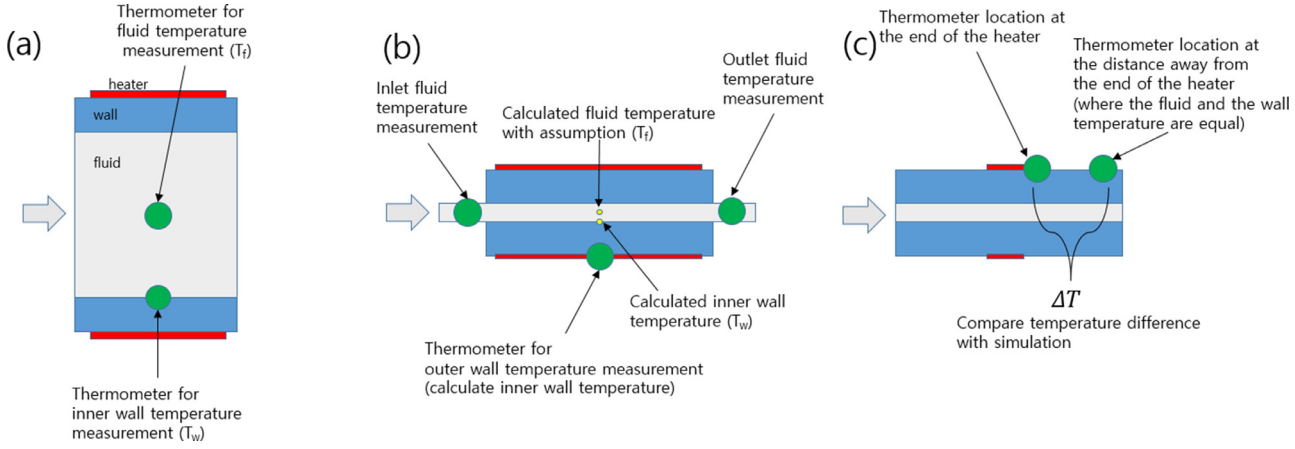

Fig. 8. Temperature measurement for the heat transfer coefficient calculation (a) macrochannel: thermometers installed in the channel. (b) microchannel: thermometers located outside channel to estimate the fluid temperature assuming a linear temperature profile, (c) proposed method for a microchannel: two thermometers, one situated at the end of the heater and the second a distance away at which the fluid and wall temperatures are equal.

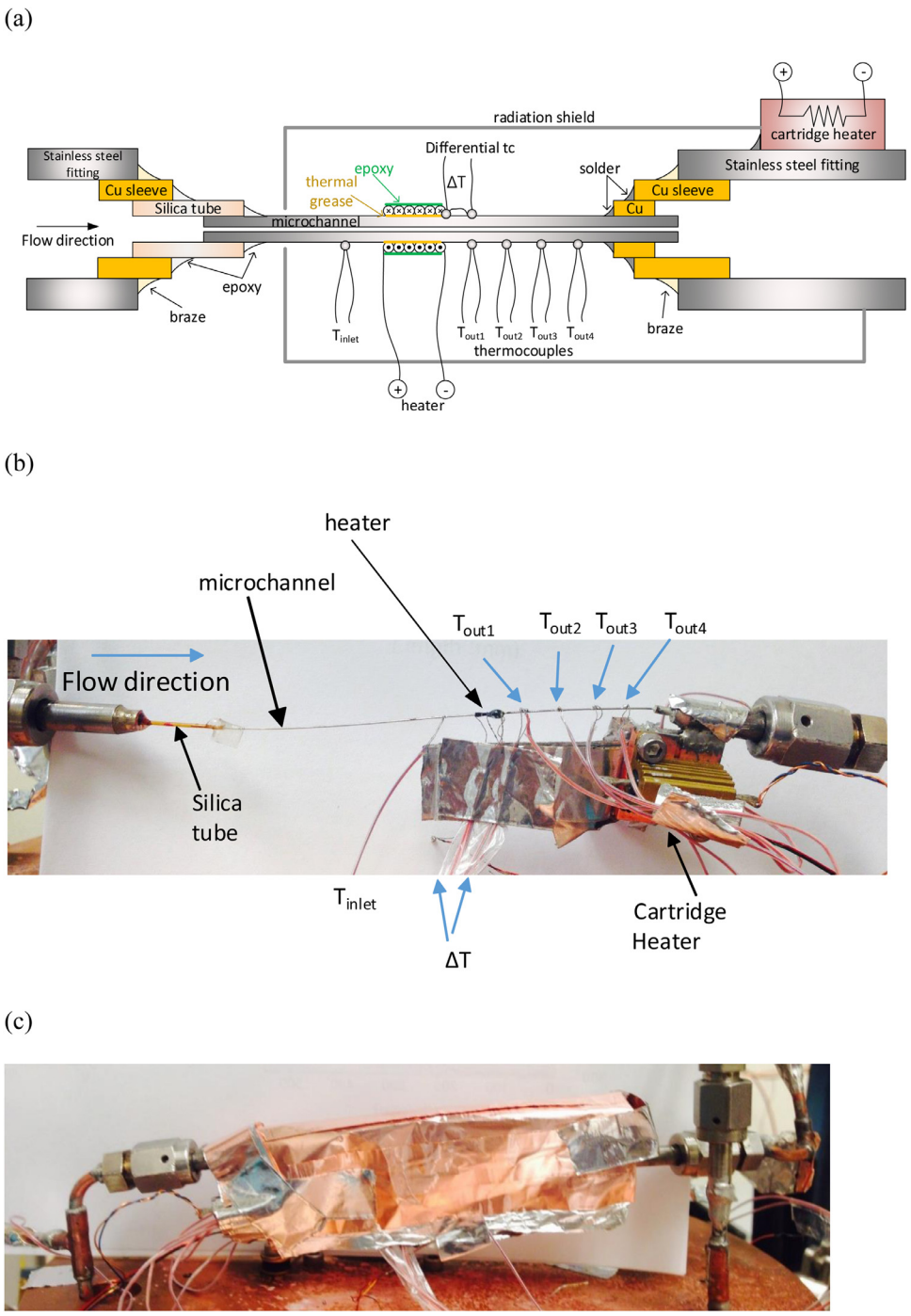

Fig. 10. (a) microchannel setup (b) picture of microchannel (c) microchannel assembly with radiation shield.

sor passes through the recuperator, and after passing through the microchannel, returns through the recuperator to the compressor. The recuperator is a custom counterflow heat exchanger fabricated with copper tubes that pre-cools the inflow gas while heating the return flow gas to ambient temperature.

The test section consists of the microchannel, a heater, a differential thermocouple, and six thermocouples. Table 3 gives the specifications of the microchannel used in this study. Fig. 10 (a) shows a close-up schematic of the test section. The microchannel is a stainless steel 304 tube. One E-type differential thermocouple was installed at the end of the heated zone and 3 mm away from the heated zone. An additional thermocouple was installed 3 mm away from the end of the heated zone to measure absolute temperature of the wall. An additional four E-type thermocouples were soldered to the tinned microchannel wall to measure the inlet and outlet temperatures. The heating wire was wound after soldering the differential thermocouple to the wall. The exterior surface of the microchannel was cleaned with acetone after soldering the thermocouples to the wall. Prior to winding the heater, thermal grease was applied to the surface of the microchannel to improve the thermal contact between the heater and the microchannel. The heater wire diameter was 120 μm. A conductive epoxy was applied to complete the assembly. The microchannel was then connected to metal gasket fittings that connect with copper tubes

Table 4
Uncertainty analysis.

Measurement	Range	Error
Temperature	77 K ~ 400 K	±0.1 K
Pressure	0 MPa ~ 1 MPa	±0.5%
Mass flow rate	0 sccm ~ 500 sccm	±0.5%
Total uncertainty		~7 %

(6.35 mm OD) in the closed loop set up. At the inlet, a silica tube (ID=450 μm, OD=660 μm) was used as a sleeve to connect with the copper tube. Epoxy was applied as a sealant. At the exit, a copper sleeve (ID=600 μm, OD=1500 μm) was used to connect with the copper tube. The wound heating-wire was electrically insulated, so there were no electrical shunts with the thermocouples. The roughness of the microchannel was not measured in this study since it has negligible effect on the laminar flow [19].

Since the metal gasket fitting has a large mass compared with the microchannel, the wall temperature of the microchannel is affected by the temperature of the metal gasket connector. To decrease the measurement error, a cartridge heater was installed at the exit connector of the microchannel. This maintains the temperature of the connector to be the same as the outlet wall temperature of the microchannel. An additional thermocouple is installed at the cartridge heater, and PID control is applied to the cartridge heater. The temperature of the metal gasket connector follows the temperature of the microchannel wall (T_{out1}). A radiation shield was attached to the outlet part of the metal gasket connector. The radiation shield surrounds the microchannel assembly without contact to the microchannel.

The test section was maintained in vacuum of 0.013 Pa (10^{-4} torr) or better to eliminate surrounding conduction. A mass flow meter was installed in the return stream to measure the flow rate of the circulating fluid. The flow rate in the closed loop is adjusted by a valve at the bypass loop near the compressor. Two pressure transducers are located at the entrance and the exit of the microchannel to measure the pressure drop across the microchannel. The heating power to the microchannel was measured from the voltage drop and current across the heating wire. A nano-voltmeter with 1 nV resolution was utilized to measure the voltage across the differential thermocouple. The temperature drop across the differential thermocouple is calculated based on the International Temperature Scale of 1990 (ITS-90) [20].

The measured temperature, pressure, flow rate, and power input to the microchannel are collected by data acquisition devices and sent to a personal computer. The data are gathered once each second and time-averaged for a minute. The uncertainty of the measured data is determined with Eq. (6), where B is the total bias error, N is the total number of data points, and S is the standard deviation of the data [21]. The value of B is provided by the manufacturer. The $t_{95\%}$ is 2.0 in this case.

$$U = \sqrt{B^2 + \left(t_{95\%}\frac{S}{\sqrt{N}}\right)} \tag{6}$$

Table 4 shows the error of the measurement and the total uncertainty of the Nusselt number. The experimental results show an uncertainty of around 7 %.

5. Result and discussion

The measurement of outlet temperature difference was carried out for different Reynolds number and heat input for the proposed microscale method. Fig. 11 (a) shows the temperature measurement at different locations along the microchannel with 70 mW heat input (symbols). Table 5 gives the results in table form. The

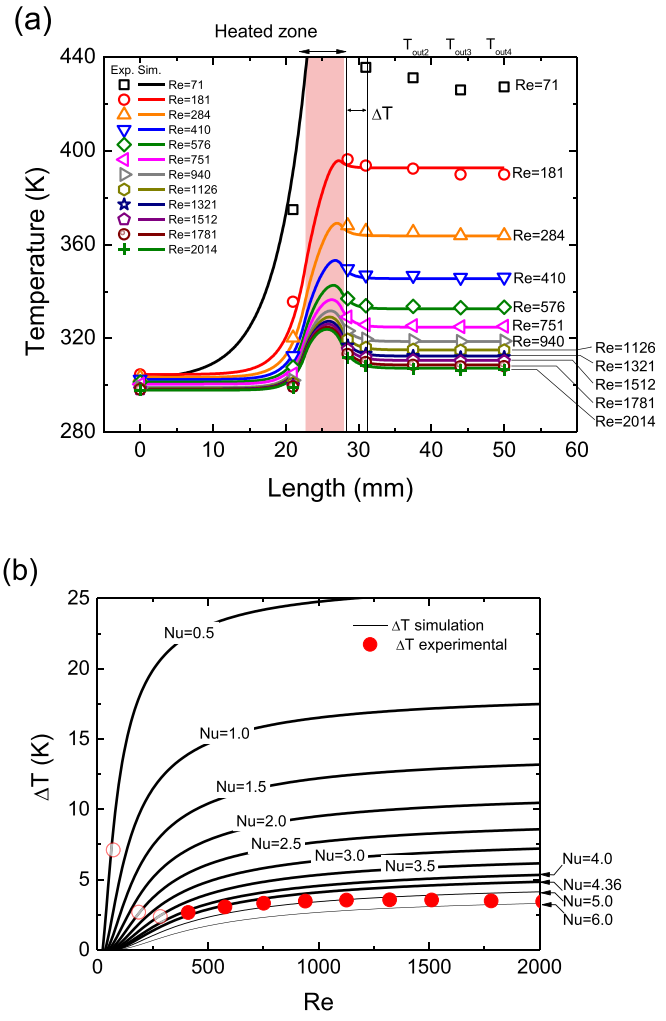

Fig. 11. 70 mW input test results: (a) comparison of wall temperature profile: experimental vs simulation (b) The temperature difference measurement, compared to Nusselt number chart.

temperature at the end of the heater shows the highest value. The outlet temperatures, T_{out2}, T_{out3}, and T_{out4} show fairly consistent values. The simulated wall temperature profile (lines) is also plotted in Fig. 11 (a). Experimental operating conditions and geometries are used in this simulation. The simulations are performed with the assumption that the Nusselt number is 4.36. The simulated wall temperature profiles at various Reynolds numbers show good agreement with the experimental values. For a low Reynolds number of 71, the simulation and the experimental results differ from each other noticeably. The temperature of the microchannel should increase up to 500 K. However, inaccuracies are found with the measurement at extremely low Reynolds flows (Re<300). The error starts to grow as the Reynolds number decreases below 284. This growth in error can be verified by checking the consistency of the outlet temperatures of the microchannel. The standard deviations of T_{out2}, T_{out3}, and T_{out4} are calculated in Table 5. The standard deviation begins to increase to more than 0.6 K when the Reynolds number approaches 300 or below. As the temperature approaches 400 K, other heat transfer mechanisms such as radiation, rather than convection to the fluid, dominate the experimental setup. Thus, it becomes difficult to control the experimental setup and maintain a perfect fluid heat transfer condition.

The comparison of the simulated wall temperature profile and the experimental values indirectly implies existence of constant Nusselt number (= 4.36) when the Reynolds number is less than

Table 5
70 mW Test results.

Location & Re #	T_{in1} (K)	T_{in2} (K)	End of heater (K)	T_{out1} (K)	T_{out2} (K)	T_{out3} (K)	T_{out4} (K)	Standard deviation for T_{out2}, T_{out3}, T_{out4} (K)
Re=71	302.00	374.92	442.77	435.67	431.23	426.03	427.34	2.20
Re=181	304.6	335.64	396.42	393.74	392.43	389.98	389.91	1.17
Re=284	303.41	320.27	368.18	365.82	365.32	363.92	363.93	0.65
Re=410	302.46	312.53	349.67	347.01	346.79	345.98	346.06	0.36
Re=576	301.38	307.79	336.96	333.91	333.65	333.13	333.26	0.22
Re=751	300.49	304.82	329.14	325.83	325.40	324.99	325.14	0.16
Re=940	299.04	302.11	323.17	319.70	319.07	318.7	318.83	0.15
Re=1126	298.61	300.90	319.615	316.07	315.27	314.86	314.98	0.17
Re=1321	298.35	300.07	316.96	313.40	312.44	311.95	312.06	0.20
Re=1512	298.23	299.75	315.27	311.72	310.65	310.14	310.25	0.22
Re=1781	297.97	298.85	311.85	308.41	307.15	306.49	306.56	0.29
Re=2014	298.13	299.30	313.354	309.85	308.66	308.07	308.14	0.26

2000. If the Nusselt number decreases with the Reynolds number, the experimental wall temperature profiles may not agree with those from the simulation.

The temperature difference on the tube between the end of the heater and 3 mm away from the heater was measured with an E-type differential thermocouple. Fig. 11 (b) shows the measurement of the temperature difference over different Reynolds numbers (indicated by solid red circles). The temperature difference decreases gradually as the Reynolds number decreases from 2000 to 300. When the Reynolds number declines below 300, the temperature difference starts to increase. However, these conditions do not follow the trend of the wall temperature profile from the numerical work. For clarity, the temperature differences for Reynolds numbers less than 300 are indicated with open red circles.

The temperature differences on the wall between a point at the end of the heater and a point 3 mm away from the heater are simulated with various Reynolds numbers and Nusselt numbers. For Nusselt numbers lower than 4.36, the temperature differences are higher. The experimental temperature differences show a similar trend with the simulation for Nu=4.36 but the data are below the Nu=4.36 line (Fig. 11 (b)). If the Nusselt number is decreased for Reynolds numbers less than about 1500, as shown in previous research [7, 8, 10], the temperature difference should increase. However, the experimental temperature differences do not indicate an increasing tendency for decreasing Reynolds number. This comparison of experimental and simulated temperature differences validates the theoretical result that the Nusselt number is constant when the Reynolds number is less than 2000 for flow in microchannels. The disagreement of temperature difference at high Reynolds numbers around 2000 may be an indication of transition to turbulent behavior of the heat transfer.

Additional experiments were carried out with 0.1 W heat input to the microchannel. Fig. 12 (a) shows the temperature measurement at similar locations on the microchannel (symbols). The Reynolds number was varied from 56 to 1824. The simulation wall profiles are again depicted as lines in the figure. The measurements and simulation show good agreement with each other for Reynolds numbers higher than 300, which is similar to that for 70 mW heat input (Fig. 11). The standard deviation of the outlet temperatures (T_{out2}, T_{out3}, and T_{out4}) are shown in Table 6. The standard deviation starts to exceed 0.6 K for Reynolds numbers less than 275, which implies that these data (below Re=275) do not represent good experimental conditions.

The solid red circles in Fig. 12 (b) show measurement results for the temperature difference between the end of the heated zone and 3 mm away from the heater. The data below a Reynolds number of 300 are shown as open red circles. Similar to results for 70 mW, at 0.1 W input the temperature differences decrease gradually for decreasing Reynolds numbers from about 500 downward. Simulated temperature differences for various Nusselt numbers are

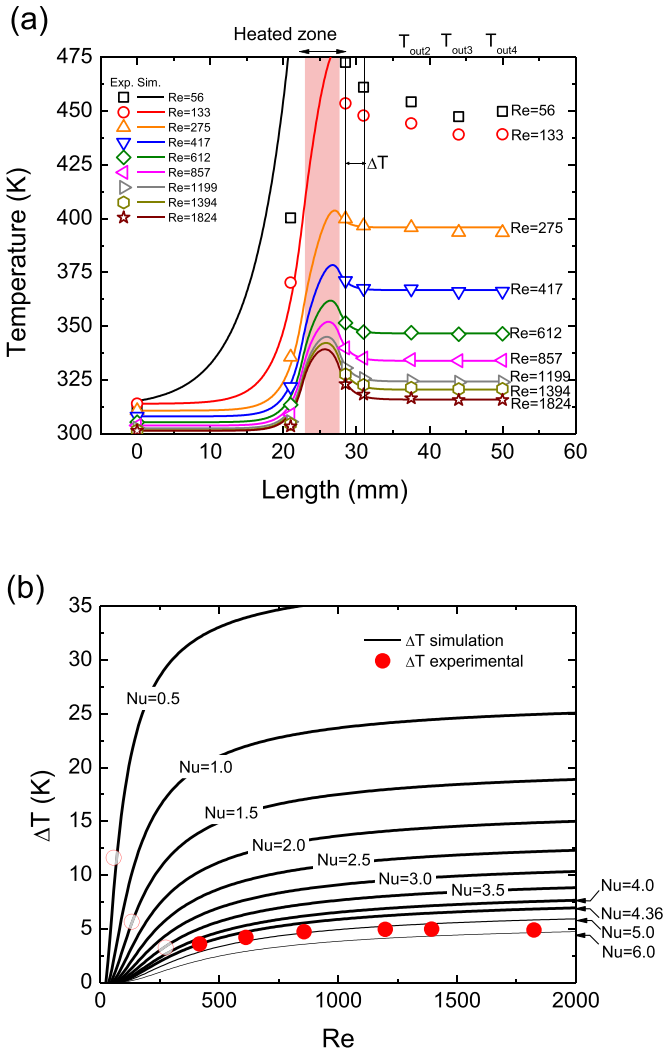

Fig. 12. 0.1 W test results (a) comparison of wall temperature profile: experimental vs simulation (b) The temperature difference measurement, compared to Nusselt number chart.

indicated in Fig. 12 (b). The experimental temperature differences do not show a decreasing trend as the Reynolds number decreases which validates that the Nusselt number is constant in the laminar flow regime.

Fig. 13 shows how the measured Nusselt numbers vary with Reynolds numbers with the new measurement technique. These data are compared to the apparent Nusselt number obtained from the traditional measurements that assume a linear fluid tempera-

Table 6
0.1W test results.

Location & Re #	T_{in1} (K)	T_{in2} (K)	End of heater (K)	T_{out1} (K)	T_{out2} (K)	T_{out3} (K)	T_{out4} (K)	Standard deviation for T_{out2}, T_{out3}, T_{out4} (K)
Re=56	312.39	400.29	472.60	461.0	454.25	447.38	449.76	2.84
Re=133	313.93	370.21	453.50	447.87	444.23	439.08	439.17	2.40
Re=275	310.77	335.67	399.86	396.62	395.80	393.64	393.56	1.03
Re=417	308.08	321.86	371.15	367.56	367.28	366.13	366.22	0.52
Re=612	305.36	313.51	351.5	347.31	346.99	346.3	346.48	0.29
Re=857	303.82	308.89	339.85	335.13	334.45	333.93	334.08	0.21
Re=1199	302.48	305.52	330.54	325.6	324.46	323.88	324.01	0.24
Re=1394	301.64	304.54	327.67	322.7	321.33	320.70	320.83	0.27
Re=1824	301.39	303.40	323.09	318.19	316.54	315.67	315.73	0.39

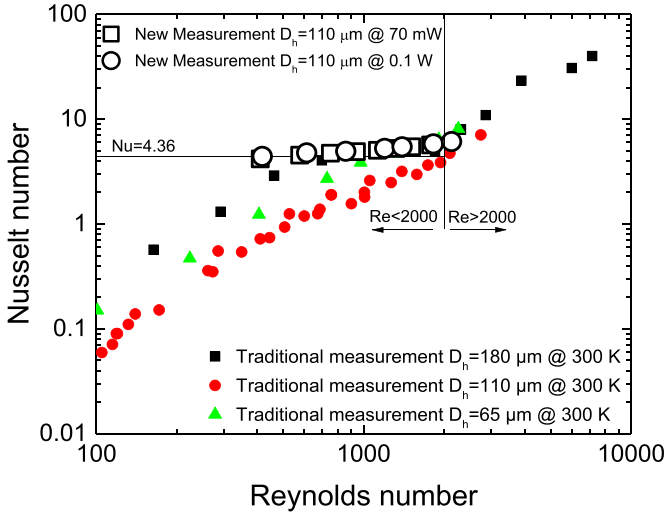

Fig. 13. Comparison of Nusselt number between the new measurement and the traditional measurement [15, 22].

ture profile [15, 22]. The new measurement technique influences the Nusselt number very little compared with the traditional measurements undertaken previously and represents nearly an order of magnitude improvement at low Reynolds number laminar flow. The Nusselt number obtained from the new measurements show a near constant value for Reynolds numbers between 300 and 2000.

6. Conclusion

In this work, a new heat transfer coefficient measurement technique for the laminar flow regime has been developed for microchannels smaller than thermometer sizes, where axial thermal conduction cannot be neglected. The method relies on the measurement of wall temperature along the heater section, and a short distance after the heater section. The measured temperature profile is correlated with that obtained from simulation using different Nusselt numbers to derive the measured Nusselt number. The axial conduction effect is accounted for in the measurements which led to a significant improvement over traditional measurement techniques. The comparison indicates that the Nusselt number in a 160 μm microchannel is independent of Reynolds number for the laminar flow regime as it is in macrochannels, at least for Reynolds numbers down to 300.

Declaration of Competing Interest

The authors whose names are listed immediately below certify that they have NO affiliations with or involvement in any organization or entity with any financial interest (such as honoraria; educational grants; participation in speakers' bureaus; membership, employment, consultancies, stock ownership, or other equity interest; and expert testimony or patent-licensing arrangements), or non-financial interest (such as personal or professional relationships, affiliations, knowledge or beliefs) in the subject matter or materials discussed in this manuscript.

Acknowledgment

We gratefully acknowledge the DARPA FPA-MCC program for funding support.

References

[1] A. Bejan, Convective heat transfer, 2013.
[2] V. Gnielinski, New equations for heat and mass transfer in the turbulent flow in pipes and channels, NASA STI/Recon Tech. Rep. A 41 (1975) 8.
[3] J.P. Abraham, E.M. Sparrow, W.J. Minkowycz, Internal-flow Nusselt numbers for the low-Reynolds-number end of the laminar-to-turbulent transition regime, Int. J. Heat Mass Transf. 54 (1) (2011) 584–588.
[4] J.P. Abraham, E.M. Sparrow, J.C.K. Tong, Heat transfer in all pipe flow regimes: laminar, transitional/intermittent, and turbulent, Int. J. Heat Mass Transf. 52 (3) (2009) 557–563.
[5] F. Dittus, L. Boelter, Heat Transfer in Automobile Radiators of the Tubular Type, Univ. California Publ. Eng. 2 (1930) 371.
[6] M. Asadi, G. Xie, B. Sunden, A review of heat transfer and pressure drop characteristics of single and two-phase microchannels, Int. J. Heat Mass Transf. 79 (2014) 34–53.
[7] P. Wu, W.A. Little, Measurement of the heat transfer characteristics of gas flow in fine channel heat exchangers used for microminiature refrigerators, Cryogenics 24 (1984) 415–420.
[8] S.Choi, R.Barron, R.Warrington, Fluid flow and heat transfer in microtubes, in: ASME DSC, 1991, pp. 123-134.
[9] X.F. Peng, G.P. Peterson, Convective heat transfer and flow friction for water flow in microchannel structures, Int. J. Heat Mass Transf. 39 (12) (1996) 2599–2608.
[10] G.L. Morini, Y. Yang, M. Lorenzini, Experimental Analysis of Gas Micro-Convection Through Commercial Microtubes, Exp. Heat Transf. 25 (3) (2012) 151–171.
[11] E.N. Sieder, G.E. Tate, Heat Transfer and Pressure Drop of Liquids in Tubes, Indust. Eng. Chem. 28 (12) (1936) 1429–1435.
[12] C.-Y. Yang, C.-W. Chen, T.-Y. Lin, S.G. Kandlikar, Heat transfer and friction characteristics of air flow in microtubes, Exp. Therm. Fluid Sci. 37 (0) (2012) 12–18.
[13] G. Maranzana, I. Perry, D. Maillet, Mini- and micro-channels: influence of axial conduction in the walls, Int. J. Heat Mass Transf. 47 (17–18) (2004) 3993–4004.
[14] T.-Y. Lin, S.G. Kandlikar, A theoretical model for axial heat conduction effects during single-phase flow in microchannels, J. Heat Transf. 134 (2) (2012) 020902.
[15] S. Baek, P.E. Bradley, R. Radebaugh, Heat transfer coefficient measurement of LN2 and GN2 in a microchannel at low Reynolds flow, Int. J. Heat Mass Transf. 127 (2018) 222–233.
[16] G. Nellis, S. Klein, Heat transfer, Cambridge University Press, 2009.
[17] S. Baek, C. Lee, S. Jeong, Effect of flow maldistribution and axial conduction on compact microchannel heat exchanger, Cryogenics 60 (2014) 49–61.
[18] E.W. Lemmon, M.L. Huber, M.O. McLinden, NIST Standard Reference Database 23: Reference Fluid Thermodynamic and Transport Properties-REFPROP, in, National Institute of Standards and Technology, Standard Reference Data Program, Gaithersburg (2010).
[19] J.B. Taylor, A.L. Carrano, S.G. Kandlikar, Characterization of the effect of surface roughness and texture on fluid flow—past, present, and future, Int. J. Therm. Sci. 45 (10) (2006) 962–968.
[20] H. Preston-Thomas, The International Temperature Scale of 1990(ITS-90), Metrologia 27 (1) (1990) 3–10.
[21] R.J. Moffat, Describing the uncertainties in experimental results, Exp. Therm. Fluid Sci. 1 (1) (1988) 3–17.
[22] S. Baek, P.E. Bradley, Single-phase ambient and cryogenic temperature heat transfer coefficients in microchannels, IOP Conf. Series Mater. Sci. Eng. 101 (2015) 012005.